COMMUNICATION

Au/Ag core–shell nanocuboids for high-efficiency organic solar cells with broadband plasmonic enhancement†

Shenghua Liu,[a] Ruibin Jiang,[b] Peng You,[a] Xingzhong Zhu,[b] Jianfang Wang[b] and Feng Yan*[a]

Although various metal nanoparticles have been used in organic photovoltaics (OPVs) for enhancing power conversion efficiencies (PCEs) based on surface plasmonic effects, no metal nanoparticles have been found to induce matchable broadband plasmonic enhancement in OPVs until now. Here, we report the introduction of Au@Ag core–shell nanocuboids (NCs) with broadband plasmonic enhancement in OPVs for the first time. The Au@Ag NCs show multimode localized surface plasmon resonance that can be tuned to match the light absorption spectra of OPVs by changing the Ag shell thickness. We find that both light scattering and near field enhancement induced by the NCs can substantially improve the device performance when the NCs are incorporated in the active layers. Under optimum conditions, the PCEs of the OPVs can be relatively improved by up to 22.8% by the NCs. The maximum average PCE of the OPVs we obtained is 10.42%, which is much higher than those of the previously reported plasmonic OPVs. This work demonstrates a convenient approach for improving the photovoltaic performance with broadband enhancement, which is applicable to not only OPVs but also many other types of solar cells.

Broader context

Plasmonic enhancement induced by metal nanoparticles is an effective approach to improve light absorption in solar cells and consequently increases the device efficiency. Although various metal nanoparticles have been introduced in organic solar cells, no metal nanoparticles have been found to induce tunable and matchable broadband plasmonic enhancement in the devices until now. In this paper, we introduced Au@Ag core–shell nanocuboids with broadband plasmonic enhancement in high-efficiency organic solar cells for the first time. The Au@Ag core–shell nanocuboids show multimode localized surface plasmon resonance that can be tuned to match the light absorption spectra of the organic solar cells by changing the particle size and the Ag shell thickness. We find that both light scattering and near field enhancement induced by the nanocuboids can substantially improve the device performance. The efficiencies of the devices are relatively improved by up to 22.8% by the nanocuboids and the maximum average efficiency of the organic solar cells obtained is 10.42%. Since the nanocuboids can be easily prepared and distributed by solution processes, our approach is cost-effective, convenient and efficient for not only organic solar cells but also many other types of solar cells.

High-efficiency and low-cost solar cells are critical technologies for alleviating the global energy crisis, in which organic photovoltaics (OPVs) have gained much attention in recent years due to their easy fabrication, light weight, low cost and mechanical flexibility.[1–6] However, the power conversion efficiencies (PCEs) of OPVs are still lower than those of inorganic counterparts due to the low carrier mobilities and short exciton diffusion lengths in organic semiconductors. Fortunately, many technologies can be conveniently integrated in OPVs to enhance their PCEs since the organic devices can be prepared by solution processes.[7–10] One promising strategy is based on the plasmonic enhancement of light absorption or light trapping by the introduction of various metallic nanoparticles (MNPs) or periodic metallic nanostructures/grating in the devices.[11–16] The localized surface plasmon resonance (LSPR) of a MNP is dependent on the particle material, size, and shape as well as its surroundings and can induce light trapping/scattering as well as near-field enhancement of electric fields.[17–21] Many types of MNPs, including Au and Ag nanoparticles with different shapes and structures such as nanosphere, nanorod, nanostar, triangular nanoprism, core–shell nanoparticle, *etc.*,[22–28] have been incorporated into the carrier transport layers[29–32] or the active layers[14,24,33–35] of OPVs to improve their performance. However, the reported MNPs used in OPVs normally show absorption enhancement in a narrow wavelength range and thus have limited effect on improving the PCEs of the devices.[13] Some groups reported the approaches of combining various types of MNPs and nanopatterned gratings in OPVs to realize the enhancement in a broader wavelength region,[25,33,36] which however led to more complicated fabrication procedures unsuitable for roll-to-roll processes and mass production.

[a] Department of Applied Physics, The Hong Kong Polytechnic University, Hung Hom, Kowloon, Hong Kong, China. E-mail: apafyan@polyu.edu.hk
[b] Department of Physics, The Chinese University of Hong Kong, Shatin, Hong Kong SAR, China

898 | *Energy Environ. Sci.*, 2016, **9**, 898–905

This journal is © The Royal Society of Chemistry 2016

Therefore, MNPs with broadband absorption enhancement matchable to the absorption spectra of OPVs are urgently needed. It is notable that a MNP can show broadband LSPR when its several plasmon modes exhibit pronounced field enhancement and light scattering in neighboring wavelength regions. A good example is Au@Ag core–shell nanocuboids (Au@Ag NCs) that exhibit broadband and tunable plasmonic enhancement due to the coexistence of longitudinal and transverse dipole modes and octupolar modes, which however have never been used in OPVs until now.[37] In this paper, we designed and tuned the thickness of the Ag shells of Au@Ag NCs to match the light absorption region of the OPVs based on polythieno[3,4-b]-thiophene/benzodithiophene:[6,6]-phenyl

C_{71}-butyric acid methyl ester (PTB7:PC$_{71}$BM) or poly[4,8-bis(5-(2-ethylhexyl)thiophen-2-yl)-benzo[1,2-b;4,5-b']dithiophene-2,6-diyl-alt-(4-(2-ethylhexyl)-3-fluorothieno[3,4-b]thiophene-)-2-carboxylate-2-6-diyl]:PC$_{71}$BM (PBDTTT-EFT:PC$_{71}$BM) and incorporated the NCs successfully in the devices (Fig. 1a and b) with pronounced PCE enhancement.[8,38] Since the plasmonic spectra of the Au@Ag NCs can be easily tuned by changing their geometric size, they are expected to be useful in many other types of OPVs and inorganic solar cells for enhancing the device performance.

Au@Ag NCs were prepared by the method reported before.[37] According to our initial simulation results to be introduced later in the paper, firstly Au nanorods with a size of 20 nm × 60 nm (diameter × length) were synthesized and then
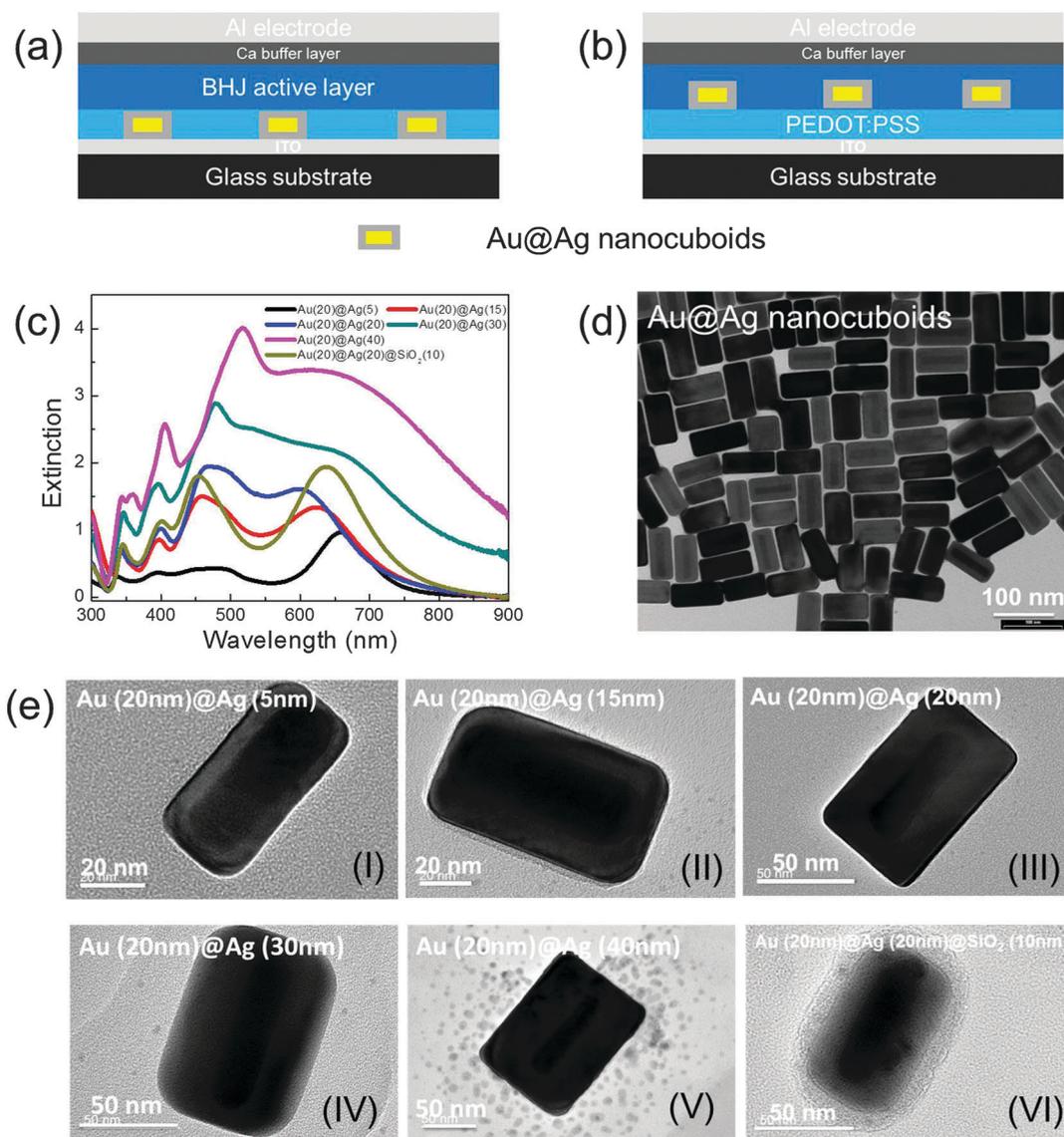

Fig. 1 Scheme of OPVs with the incorporation of Au@Ag NCs in the (a) PEDOT:PSS layer and (b) bulk heterojunction (BHJ) active layer. (c) Extinction spectra of Au@Ag NCs in aqueous solutions and Au@Ag@SiO$_2$ NCs in an ethanol solution. All samples have the same concentration of NCs in the solutions. The Au (20 nm)@Ag (5 nm), Au (20 nm)@Ag (15 nm), Au (20 nm)@Ag (20 nm), Au (20 nm)@Ag (30 nm) and Au (20 nm)@Ag (40 nm) NCs have the same diameter of Au rod (20 nm) and different Ag shell thicknesses of 5, 15, 20, 30 and 40 nm, respectively. (d) TEM images of Au (20 nm)@Ag (20 nm) NCs. (e) TEM images of individual Au@Ag NCs with different Ag shell thicknesses in (I–V) and an individual Au@Ag@SiO$_2$ NC in (VI).

the Ag shell was coated on the surface in solution, forming a cuboidal shape with rectangular edges and vertices. It is notable that the LSPR behavior of the Au/Ag NCs can be easily tuned by controlling the Ag shell thickness. Fig. 1c shows the extinction spectra of the Au@Ag NCs in aqueous solutions with the same NC concentration (2.27×10^{-10} M) but different Ag shell thicknesses ($\sim 5, 15, 20, 30, 40$ nm). The lowest-energy peak appearing at around 650 nm belongs to the longitudinal dipole plasmon mode. The second lowest-energy peak at around 500 nm corresponds to the transverse dipolar mode. The two other higher-energy peaks can be ascribed to octupolar plasmon modes.[37] With the increase of the Ag shell thickness, the peak height increases due to stronger plasmonic enhancement induced by Ag than Au. The extinction spectra for the wavelengths from 350 nm to 750 nm can fit the light absorption region of the studied OPVs very well. We also need to notice that the extinction spectra may show red shifts when the NCs are incorporated in OPVs since the refractive indices of organic semiconductors are higher than that of water. This effect will be addressed later in this paper.

Fig. 1d shows the TEM image of a class of Au@Ag NCs (Ag shell thickness: ~ 20 nm) with rather uniform sizes. The TEM images of NCs with different Ag shell thicknesses (5, 15, 20, 30 and 40 nm) are shown in Fig. 1e with higher resolution. Au nanorods can be observed in the center of each NC with a uniform coverage of Ag. We averaged the overall length, width and Ag shell thickness of each type of NC. Over 30 samples were measured for each group from the TEM images. The Au cores of all particles have a very similar size (20 ± 3 nm in diameter, 60 ± 6 nm in length), while the Ag shells determined from the TEM images show five different thicknesses of 5 ± 1, 15 ± 2, 20 ± 2, 30 ± 3, and 40 ± 5 nm in average.

As shown in Fig. 1a, OPVs based on PTB7:PC$_{71}$BM with a conventional structure of ITO/PEDOT:PSS/PTB7:PC$_{71}$BM/Ca/Al were prepared.[1,8] We fabricated five groups of devices with the incorporation of Au@Ag NCs with different shell thicknesses. In each group, a NC solution was added into PEDOT:PSS solutions with different volume ratios and PEDOT:PSS films with different densities of NCs were prepared by coating the mixed solutions on substrates. As a result, the NCs were embedded in the PEDOT:PSS layers in the devices with the structure shown in Fig. 1a. Control devices without NCs were also prepared under the same conditions in each group.

The representative J–V characteristics of the devices of each group are shown in Fig. 2a–c and Fig. S1 in the ESI.† We can find that the incorporation of Au@Ag NCs into each group can increase the short-circuit current densities (J_{sc}) and PCEs of the devices. Approximately 5 vol% addition of the NC solution in PEDOT:PSS solution can lead to the best result in each group. The detailed photovoltaic parameters including the open-circuit voltage (V_{oc}), J_{sc}, fill factor (FF), PCE and relative PCE enhancement are summarized in Tables S1–S5 in the ESI.† In general, the average efficiencies of each group of OPVs show the same relationship with the concentration of NCs. The PCE initially increases with the increase of the added NC solution from 1 to 5 vol% and then decreases gradually with the increase

of the addition level up to 20 vol%. At the optimum addition level of 5 vol%, the average PCEs of the five groups of devices with Ag shell thicknesses of 5, 15, 20, 30 and 40 nm are 8.46%, 8.52%, 8.85%, 8.69% and 8.29%, respectively, demonstrating the maximum relative PCE enhancement of 11.7% (Ag shell thickness: 20 nm) in comparison with control devices.

Comparing the devices from different groups, we can find that NCs with increasing Ag shell thicknesses up to 20 nm can lead to greater improvement, which is consistent with the increasing values of the extinction spectra of the NCs shown in Fig. 1c. However, for the NCs with the shell thicknesses larger than 30 nm, the enhancement becomes less pronounced, which can be attributed to the two possible reasons. First, too big NCs may reflect light and influence light transmission across the PEDOT:PSS film. Second, the increased surface roughness of the PEDOT:PSS film induced by the larger NCs may change the morphology of the active layer in the OPV and may degrade the device performance.

The PCE enhancement can be mainly attributed to the increase of J_{sc}, which is also reflected by the improvement of EQE in the whole wavelength region (see ESI,† Fig. S2). The champion device shows V_{oc} of 0.745 V, J_{sc} of 18.9 mA cm^{-2}, FF of 64.3%, and efficiency of 9.06%, which is 14.4% higher than that of the control device. However, a further increase of the NC density in the OPVs inversely decreases the PCEs due to the obvious degradation of J_{sc} because of the influence of light transmission by NCs in the device.

For each group, the enhanced EQE spectrum (ΔEQE) of the champion device relative to its control device is presented in Fig. 2d. In the wavelength region around 500 nm, the pronounced enhancement is due to the transverse dipole mode that is very sensitive to the Ag shell thickness as shown in Fig. 1c.[37] So the NCs with 5 nm thick Ag shells show no enhancement in EQE in this region. In the wavelength region around 700 nm, the improvement of EQE can be attributed to the longitudinal dipole mode, which also increases with the increase of the Ag shell thickness from 5 nm to 20 nm.

To better understand the effect of the Au@Ag NCs embedded in the PEDOT:PSS layer, a PEDOT:PSS thin film with the NCs (Ag shell thickness: 20 nm & addition level: 5 vol%) was characterized under Raman spectroscopy. We find that the Raman peaks of the PEDOT:PSS film are enhanced by about 100% by the NCs (see ESI,† Fig. S3a),[39] suggesting an obvious plasmonic near-field enhancement of the NCs. The introduction of the NCs can also increase the light absorption of the PEDOT:PSS film due to the LSPR of the NCs in the PEDOT:PSS film (see ESI,† Fig. S4). A PEDOT:PSS thin film prepared with the above condition was characterized under TEM to obtain the NC distribution in the film. As shown in the TEM image in Fig. S3c (ESI†), the distribution of Au@Ag NCs is relatively uniform in the PEDOT:PSS layer without particle aggregation and its average density is about 4.5 NC/μm^2. Considering that the cross-sectional area of each NC is about 60 nm $\times$ 100 nm, we can estimate that the occupation area of the NCs is only $\sim 2.7\%$ relative to the area of the PEDOT:PSS film.

900 | *Energy Environ. Sci.*, 2016, **9**, 898–905
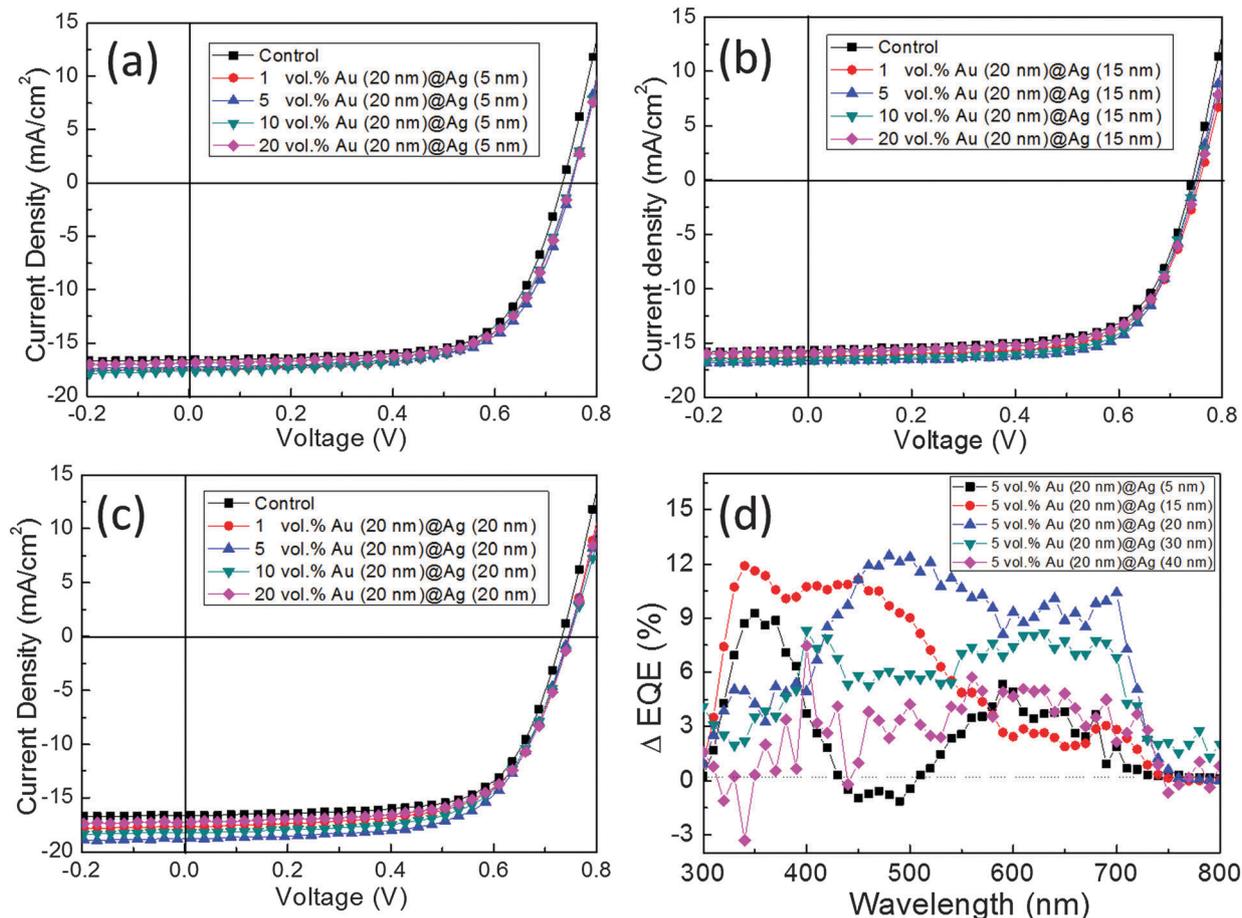
This journal is © The Royal Society of Chemistry 2016

Fig. 2 Current density−voltage (J−V) curves of the best control device and the OPVs with various addition levels (1, 5, 10, 20 vol%) of (a) Au (20 nm)@Ag (5 nm), (b) Au (20 nm)@Ag (15 nm), and (c) Au (20 nm)@Ag (20 nm) NCs. (d) EQE enhancement (ΔEQE) of the OPVs with the addition level of 5 vol% of Au@Ag NCs with different Ag shell thicknesses.

Three-dimensional finite-difference time-domain (FDTD) simulation was carried out to better understand the plasmonic enhancement in the OPVs by the NCs.[37] As shown in Fig. S5 in the ESI,† the electric field intensity around the NCs is substantially enhanced. However, because the NCs are located in the PEDOT layer, the enhanced electric field around the NCs cannot obviously affect the light absorption of the active layer. So the major reason for the improved performance is the light scattering effect as demonstrated in the simulated scattering spectrum in Fig. S6 (ESI†). We can find that, for the same concentration of NCs in the PEDOT:PSS layer, the NCs with larger shell thicknesses can lead to a stronger and broader light scattering spectrum, which is consistent with the absorption spectra shown in Fig. 1c.

To further improve the device performance by near-field enhancement of LSPR, the NCs were incorporated in the active layers of the OPVs by coating them on the surface of PEDOT:PSS films before the deposition of PTB7:PC₇₁BM.[40] So the devices have the structure of ITO/PEDOT:PSS/Au@Ag NCs:PTB7:PC₇₁BM/Ca/Al shown in Fig. 1b. Since the average thicknesses of the NCs and the organic active layers are 60 nm and 90 nm, respectively, the NCs are totally embedded in the

active layers of the OPVs. However, the PCE was dramatically decreased after the introduction of the Au@Ag NCs in the active layer, as shown in Fig. S7 in the ESI.† The poor result can be ascribed to the non-radiative exciton quenching on the bare Ag surface due to the direct contact between the silver shell and the active layer.[29,35] To overcome this negative effect, NCs were coated with an insulating silica layer, as shown in Fig. 1e. The SiO₂ thickness was controlled to be about 10 nm. Due to the higher refractive index of SiO₂ than that of water, it is reasonable to find that the SiO₂-coated Au@Ag (Au@Ag@SiO₂) NCs exhibit a red shift of the longitudinal resonance peak in Fig. 1c.

OPVs with NCs embedded in the active layers were prepared with the standard fabrication conditions in a glovebox.[8] The density of the NCs coated on the PEDOT:PSS layer was controlled by changing the spin coating speed of the NC solution. It is notable that the PCEs of the devices were dramatically enhanced by the Au@Ag@SiO₂ NCs especially under the optimum condition with the spin coating speed of ∼2000 rpm (see the ESI,† Fig. S8). The coated Au@Ag@SiO₂ NCs were characterized under a scanning electron microscope (SEM) and a relatively uniform distribution of the NCs on the PEDOT:PSS film was observed. At the coating speed of 2000 rpm, the average
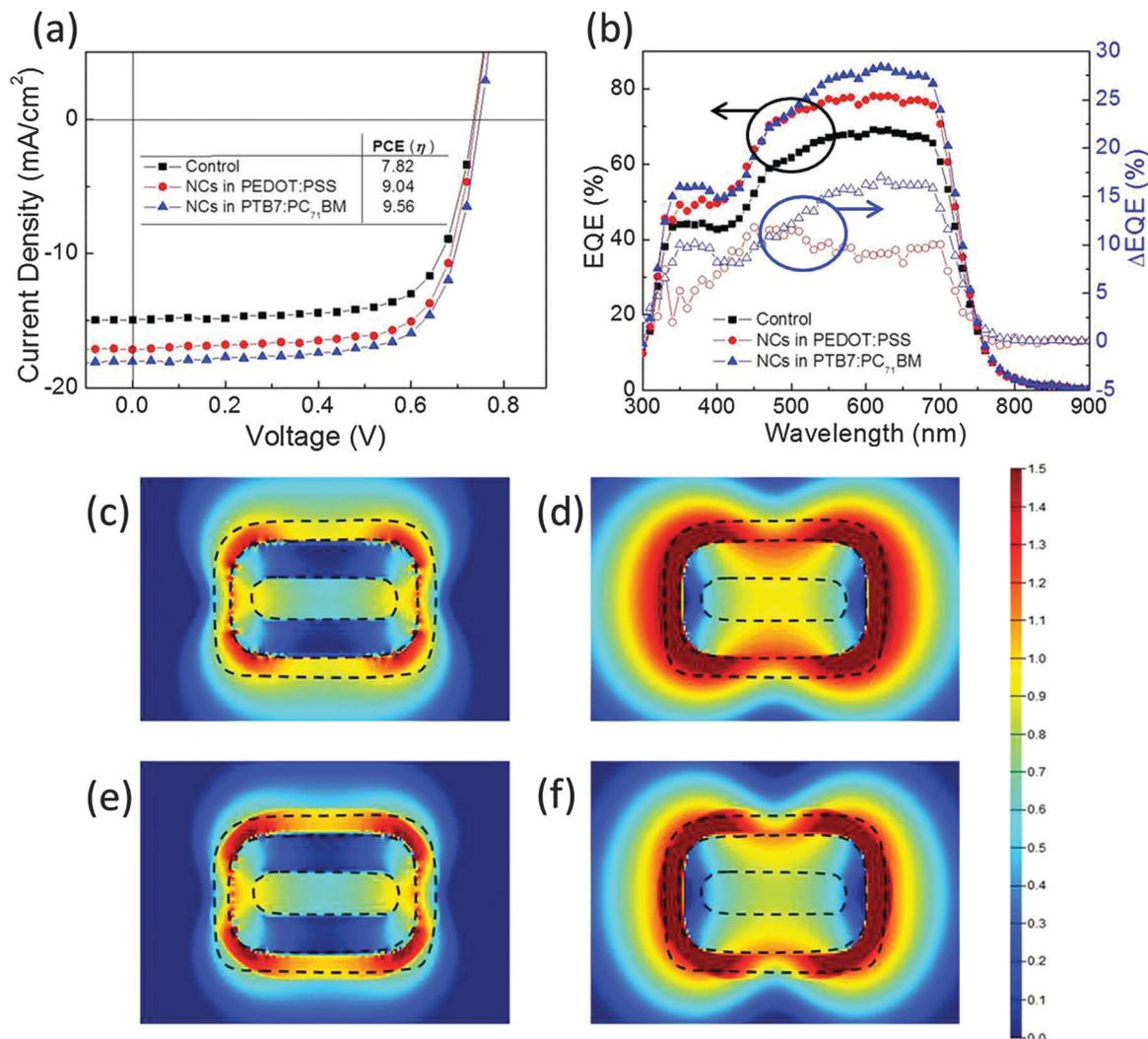
Fig. 3 (a) J–V, (b) EQE (solid symbols) and EQE enhancement (ΔEQE) (open symbols) curves of PTB7:PC$_{71}$BM-based OPVs with Au@Ag@SiO$_2$ NCs in the PEDOT:PSS layer or the active layer. (c and d) Simulated enhancement distribution of the electric field intensity for Au@Ag@SiO$_2$ NCs in PEDOT:PSS with (c) the transverse dipole mode and (d) the longitudinal dipole mode at the resonance wavelengths of 492 nm and 621 nm, respectively. (e and f) Simulated electric field enhancement for Au@Ag@SiO$_2$ NCs in PTB7:PC$_{71}$BM with (e) the transverse dipole mode and (f) longitudinal dipole mode at the resonance wavelengths of 513 nm and 691 nm, respectively. The dashed lines show the boundaries between two different media. The enhancements of the electric field intensity are presented at the logarithmic scale.

density is 2.7 NC/μm^2, which is similar to the density of NCs embedded in PEDOT:PSS layers (Fig. S9, ESI†). We also find that the incorporation of the NCs in the active layer with the same density can obviously increase the light absorption of the film (see ESI,† Fig. S10)

Fig. 3a shows the J–V curves of the OPVs with Au@Ag@SiO$_2$ NCs embedded in the active layers. For comparison, OPVs with Au@Ag@SiO$_2$ NCs embedded in PEDOT:PSS layers and the control devices without NCs were also prepared at the optimum concentrations and the corresponding J–V curves are presented in the same figure. V_{oc} and FF of the three devices are very similar, while J_{sc} and PCE of the devices with NCs are obviously improved in comparison with the control device. The photovoltaic parameters of the three types of devices are summarized in Table 1. For each condition, at least six devices were fabricated to obtain the average PCE. The devices with the NCs embedded in the

PEDOT:PSS layer exhibit an average PCE of 8.84% with 14.5% relative enhancement, which mainly resulted from the increase in J_{sc} (16.98 mA cm^{-2}). A more pronounced effect can be observed in the devices with the NCs embedded in the active layers, which show an average PCE of 9.48% and a relative enhancement of 22.8% due to the improvement of J_{sc} (18.10 mA cm^{-2}).

EQE measurements of the OPVs were then conducted to illuminate the improvement of the device performance, as shown in Fig. 3b. It is obvious that the EQEs of the two devices are dramatically improved in the visible region by the NCs. More importantly, the device with the NCs embedded in the active layer shows higher EQE than the device with the NCs in the PEDOT:PSS layer, presumably due to stronger near field enhancement in the former. To better understand the LSPR of the NCs in the OPVs, the electric fields for different resonant

Table 1 Summary of photovoltaic performance of devices based on PTB7:PC$_{71}$BM with different locations of Au@Ag@SiO$_2$ NCs

Devices		J_{SC} (mA cm^{-2})	V_{oc} (V)	FF (%)	PCE (%)	Relative PCE enhancement (%)
Control	Average	14.85	0.738	70.4	7.72 ± 0.08	—
NCs in PEDOT:PSS	Average	16.98	0.742	70.1	8.84 ± 0.14	14.5 ± 1.9
	Best	17.15	0.738	71.4	9.04	17.1
NCs in PTB7:PC$_{71}$BM	Average	18.10	0.741	70.7	9.48 ± 0.05	22.8 ± 0.6
	Best	18.07	0.747	70.8	9.56	23.8

modes, including longitudinal and transverse dipole modes, were simulated by the FDTD method. As shown in Fig. 3c–f, the resonance wavelengths are different for the NCs in PEDOT:PSS and PTB7:PC$_{71}$BM layers due to the different refractive indices of the surrounding mediums (see the ESI,† Fig. S11).[41,42] For the longitudinal mode, the enhanced electric field was extended into the organic medium (PEDOT:PSS or PTB7:PC$_{71}$BM) for tens of nanometers from the SiO$_2$ surface, which may greatly improve the light absorption of the active layer, while the transverse mode has a much narrower distribution of electric field in the organic part and thus may play a less important role in improving the device performance than the former. We do find that the enhancement of EQE in the wavelength region of 550–750 nm is more pronounced in the device with the NCs in the active layer, which can be attributed to the effect of the longitudinal plasmon mode of the NCs. Therefore, the incorporation of NCs in the active layer can dramatically improve the light absorption of the active layer by both light scattering and near field enhancement. It is noteworthy that the relative enhancement of the device efficiency (22.8%) we obtained is the highest in the previously reported high-efficiency plasmonic OPVs (PCE >8%) due to the rational design of both the NCs and the device structure (see ESI,† Table S6).

To obtain OPVs with higher efficiencies, another type of donor PBDTTT-EFT, which has a broader light absorption region than that of PTB7, was used in the devices. The OPVs based on PBDTTT-EFT:PC$_{71}$BM were fabricated with the addition of Au@Ag@SiO$_2$ NCs in either the PEDOT:PSS layer or the active layer.[8] Fig. 4a shows the J–V curves of the OPVs with the incorporation of Au@Ag@SiO$_2$ NCs in different layers. The photovoltaic parameters of the devices are summarized in Table 2. The PBDTTT-EFT:PC$_{71}$BM control devices without NCs gave an average V_{oc} of 0.789 V, J_{sc} of 17.32 mA cm^{-2}, FF of 66.8% and an average PCE of 9.13%, which are comparable with the performances reported in the literature.[8,38,43] After the introduction of 5 vol% of Au@Ag@SiO$_2$ NC solution in the PEDOT:PSS solution, the devices show the average V_{oc}, J_{sc}, and FF of 0.784 V, 18.33 mA cm^{-2} and 68.5%, respectively, which result in an obvious increase of the average PCE to 9.85%. For the OPVs with the NCs embedded in the active layer, more significant enhancement in J_{sc} is obtained, leading to a higher average PCE of 10.42 ± 0.12% and the highest PCE that can be obtained is 10.59%. The relative enhancement of the average PCE of the devices induced by the NCs is about 14.1%.

The J_{sc} improvement is also consistent with EQE enhancement, as shown in Fig. 4b. In comparison with the control device, the EQEs of the two devices are enhanced by NCs in the whole wavelength region. Similar to the devices based on PTB7:PC$_{71}$BM, the NCs embedded in the active layers can induce more pronounced EQE improvement than the NCs in PEDOT:PSS layers because the near field plasmonic enhancement around the NCs can increase the light absorption of the active layers in the former case. This effect can be clearly observed in the EQE spectra in the wavelength region from 550 nm to 750 nm, which
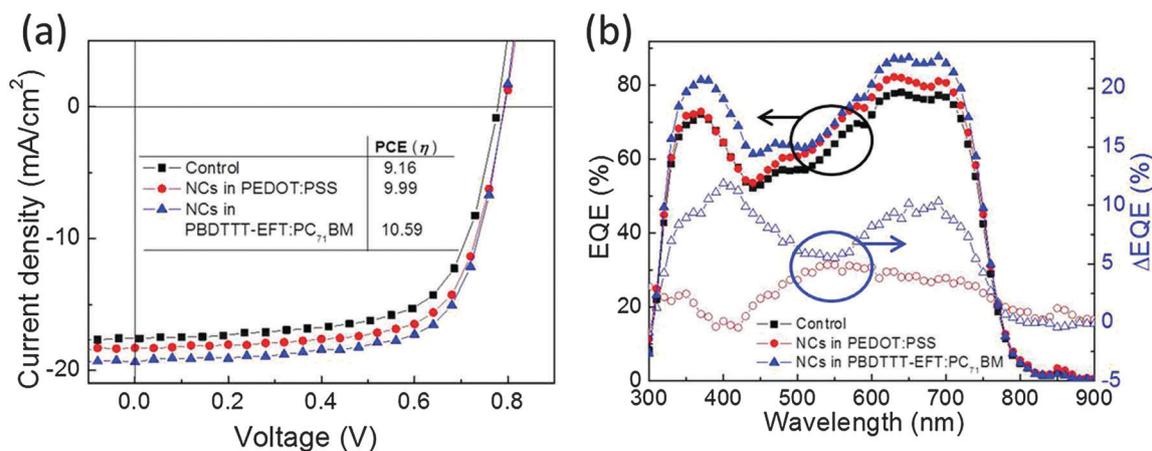

Fig. 4 (a) J–V, (b) EQE (solid symbols) and EQE enhancement (ΔEQE) (open symbols) curves of PBDTTT-EFT:PC$_{71}$BM-based OPVs with the Au@Ag@SiO$_2$ NCs embedded in PEDOT:PSS or PBDTTT-EFT:PC$_{71}$BM layers.

This journal is © The Royal Society of Chemistry 2016

Energy Environ. Sci., 2016, **9**, 898–905 | 903

Table 2 Summary of the photovoltaic performance of OPVs based on PBDTTT-EFT:PC$_{71}$BM with different locations of Au@Ag@SiO$_2$ NCs

Devices		J_{SC} (mA cm^{-2})	V_{oc} (V)	FF (%)	PCE (%)	Relative PCE enhancement (%)
Control	Average	17.32	0.789	66.8	9.13 ± 0.08	—
NCs in PEDOT:PSS	Average	18.33	0.784	68.5	9.85 ± 0.10	7.9 ± 1.1
	Best	18.30	0.793	69.1	9.99	9.4
NCs in PBDTTT-EFT:PC$_{71}$BM	Average	19.21	0.788	68.8	10.42 ± 0.12	14.1 ± 1.3
	Best	19.39	0.792	69.1	10.59	16.0

corresponds to the resonance peak of the longitudinal mode of the NCs in the active layer. In this wavelength region, the EQE enhancement by the NCs in the active layer is much larger than that induced by the NCs in the PEDOT:PSS layer because of the enhanced electric field in the active layer by the NCs in the former case. The improved light absorption of the active layer was also confirmed by the UV-visible absorption spectra of a PBDTTT-EFT:PC$_{71}$BM film with embedded NCs (see ESI,† Fig. S10).

Conclusions

In summary, Au@Ag NCs were successfully used in OPVs to enhance the device performance in a broad wavelength region for the first time. The LSPR behavior of Au@Ag NCs was finely tuned by controlling the Ag shell thickness to match the light absorption spectra of the active layers of the OPVs and the optimum thickness of the Ag shell was found to be about 20 nm. To prohibit carrier recombination on the Ag surface, the Au@Ag NCs were coated with a 10 nm-thick SiO$_2$ layer. The Au@Ag@SiO$_2$ NCs were incorporated in the OPVs by embedding them in either the PEDOT:PSS layer or the active layer and showed more pronounced enhancement of PCEs in the latter case due to the more significant enhancement of electric field in the active layer. The average PCE of the OPVs based on PTB7:PC$_{71}$BM was improved from 7.72% to 9.48% by the Au@Ag@SiO$_2$ NCs embedded in the active layer, resulting in the relative enhancement of 22.8%. Similarly, the NCs lead to the increase of the average PCE of PBDTTT-EFT:PC$_{71}$BM-based OPVs from 9.13% to 10.42%, demonstrating the first plasmonic OPV with the efficiency higher than 10%. Due to the broadband enhancement of the NCs and the facile solution processes of the devices, the relative enhancement in the PCEs of our OPVs induced by the NCs is much higher than those induced by the MNPs reported before. This work provides a novel approach to realize high-performance plasmonic solar cells including not only OPVs but also many other new generation thin film solar cells. Since the NCs can be easily prepared and coated by solution processes, this technology is also compatible with the roll-to-roll process of OPVs for mass production.

Acknowledgements

Notes and references

1 Y. Liang, Z. Xu, J. Xia, S.-T. Tsai, Y. Wu, G. Li, C. Ray and L. Yu, *Adv. Mater.*, 2010, **22**, 135.
2 G. Li, R. Zhu and Y. Yang, *Nat. Photonics*, 2012, **6**, 153.
3 J. You, L. Dou, K. Yoshimura, T. Kato, K. Ohya, T. Moriarty, K. Emery, C.-C. Chen, J. Gao, G. Li and Y. Yang, *Nat. Commun.*, 2013, **4**, 1446.
4 Z. K. Liu, J. H. Li and F. Yan, *Adv. Mater.*, 2013, **25**, 4296.
5 Y. Liu, J. Zhao, Z. Li, C. Mu, W. Ma, H. Hu, K. Jiang, H. Lin, H. Ade and H. Yan, *Nat. Commun.*, 2014, **5**, 5293.
6 Z. C. He, B. Xiao, F. Liu, H. B. Wu, Y. Yang, S. Xiao, C. Wang, T. P. Russell and Y. Cao, *Nat. Photonics*, 2015, **9**, 174.
7 J.-D. Chen, C. Cui, Y.-Q. Li, L. Zhou, Q.-D. Ou, C. Li, Y. Li and J.-X. Tang, *Adv. Mater.*, 2015, **27**, 1035.
8 S. H. Liu, P. You, J. H. Li, J. Li, C.-S. Lee, B. S. Ong, C. Surya and F. Yan, *Energy Environ. Sci.*, 2015, **8**, 1463.
9 Z. K. Liu, S. P. Lau and F. Yan, *Chem. Soc. Rev.*, 2015, **44**, 5638.
10 Z. K. Liu, J. H. Li, Z. H. Sun, G. Tai, S. P. Lau and F. Yan, *ACS Nano*, 2011, **6**, 810.
11 D. H. Wang, K. H. Park, J. H. Seo, J. Seifter, J. H. Jeon, J. K. Kim, J. H. Park, O. O. Park and A. J. Heeger, *Adv. Energy Mater.*, 2011, **1**, 766.
12 D. D. S. Fung, L. Qiao, W. C. H. Choy, C. Wang, W. E. I. Sha, F. Xie and S. He, *J. Mater. Chem.*, 2011, **21**, 16349.
13 H. A. Atwater and A. Polman, *Nat. Mater.*, 2010, **9**, 205.
14 W.-J. Yoon, K.-Y. Jung, J. Liu, T. Duraisamy, R. Revur, F. L. Teixeira, S. Sengupta and P. R. Berger, *Sol. Energy Mater. Sol. Cells*, 2010, **94**, 128.
15 Q. Gan, F. J. Bartoli and Z. H. Kafafi, *Adv. Mater.*, 2013, **25**, 2385.
16 J. Yang, J. You, C.-C. Chen, W.-C. Hsu, H.-R. Tan, X. W. Zhang, Z. Hong and Y. Yang, *ACS Nano*, 2011, **5**, 6210.
17 X. Li, W. C. H. Choy, H. Lu, W. E. I. Sha and A. H. P. Ho, *Adv. Funct. Mater.*, 2013, **23**, 2728.
18 J. A. Schuller, E. S. Barnard, W. Cai, Y. C. Jun, J. S. White and M. L. Brongersma, *Nat. Mater.*, 2010, **9**, 193.
19 K. L. Kelly, E. Coronado, L. L. Zhao and G. C. Schatz, *J. Phys. Chem. B*, 2002, **107**, 668.
20 X. Lu, M. Rycenga, S. E. Skrabalak, B. Wiley and Y. Xia, *Annu. Rev. Phys. Chem.*, 2009, **60**, 167.
21 M. Rycenga, C. M. Cobley, J. Zeng, W. Li, C. H. Moran, Q. Zhang, D. Qin and Y. Xia, *Chem. Rev.*, 2011, **111**, 3669.

22 J.-L. Wu, F.-C. Chen, Y.-S. Hsiao, F.-C. Chien, P. Chen, C.-H. Kuo, M. H. Huang and C.-S. Hsu, *ACS Nano*, 2011, **5**, 959.

23 A. P. Kulkarni, K. M. Noone, K. Munechika, S. R. Guyer and D. S. Ginger, *Nano Lett.*, 2010, **10**, 1501.

24 H. Choi, J.-P. Lee, S.-J. Ko, J.-W. Jung, H. Park, S. Yoo, O. Park, J.-R. Jeong, S. Park and J. Y. Kim, *Nano Lett.*, 2013, **13**, 2204.

25 L. Lu, Z. Luo, T. Xu and L. Yu, *Nano Lett.*, 2012, **13**, 59.

26 H. Choi, S.-J. Ko, Y. Choi, P. Joo, T. Kim, B. R. Lee, J.-W. Jung, H. J. Choi, M. Cha, J.-R. Jeong, I.-W. Hwang, M. H. Song, B.-S. Kim and J. Y. Kim, *Nat. Photonics*, 2013, **7**, 732.

27 H. C. Chen, S.-W. Chou, W.-H. Tseng, I. W. P. Chen, C. C. Liu, C. Liu, C. L. Liu, C. H. Chen, C. I. Wu and P.-T. Chou, *Adv. Funct. Mater.*, 2012, **22**, 3975.

28 D. Kozanoglu, D. H. Apaydin, A. Cirpan and E. N. Esenturk, *Org. Electron.*, 2013, **14**, 1720.

29 M. Heo, H. Cho, J.-W. Jung, J.-R. Jeong, S. Park and J. Y. Kim, *Adv. Mater.*, 2011, **23**, 5689.

30 X. Yang, C.-C. Chueh, C.-Z. Li, H.-L. Yip, P. Yin, H. Chen, W.-C. Chen and A. K. Y. Jen, *Adv. Energy Mater.*, 2013, **3**, 666.

31 S.-W. Baek, J. Noh, C.-H. Lee, B. Kim, M.-K. Seo and J.-Y. Lee, *Sci. Rep.*, 2013, **3**, 01726.

32 S.-W. Baek, G. Park, J. Noh, C. Cho, C.-H. Lee, M.-K. Seo, H. Song and J.-Y. Lee, *ACS Nano*, 2014, **8**, 3302.

33 X. Li, W. C. H. Choy, L. Huo, F. Xie, W. E. I. Sha, B. Ding, X. Guo, Y. Li, J. Hou, J. You and Y. Yang, *Adv. Mater.*, 2012, **24**, 3046.

34 D. H. Wang, D. Y. Kim, K. W. Choi, J. H. Seo, S. H. Im, J. H. Park, O. O. Park and A. J. Heeger, *Angew. Chem., Int. Ed.*, 2011, **50**, 5519.

35 V. Janković, Y. Yang, J. You, L. Dou, Y. Liu, P. Cheung and J. P. Chang, *ACS Nano*, 2013, **7**, 3815.

36 X. Li, X. Ren, F. Xie, Y. Zhang, T. Xu, B. Wei and W. C. H. Choy, *Adv. Opt. Mater.*, 2015, **3**, 1220.

37 R. Jiang, H. Chen, L. Shao, Q. Li and J. Wang, *Adv. Mater.*, 2012, **24**, OP200.

38 W. Huang, E. Gann, L. Thomsen, C. Dong, Y.-B. Cheng and C. R. McNeill, *Adv. Energy Mater.*, 2015, **5**, 1401259.

39 M. Stavytska-Barba and A. M. Kelley, *J. Phys. Chem. C*, 2010, **114**, 6822.

40 J. C. Ostrowski, A. Mikhailovsky, D. A. Bussian, M. A. Summers, S. K. Buratto and G. C. Bazan, *Adv. Funct. Mater.*, 2006, **16**, 1221.

41 K. Fehse, K. Walzer, K. Leo, W. Lövenich and A. Elschner, *Adv. Mater.*, 2007, **19**, 441.

42 Z. He, C. Zhong, S. Su, M. Xu, H. Wu and Y. Cao, *Nat. Photonics*, 2012, **6**, 591.

43 S. Zhang, L. Ye, W. Zhao, D. Liu, H. Yao and J. Hou, *Macromolecules*, 2014, **47**, 4653.

This journal is © The Royal Society of Chemistry 2016

Energy Environ. Sci., 2016, **9**, 898–905 | **905**